Journal of Materials Chemistry C

Accepted Manuscript

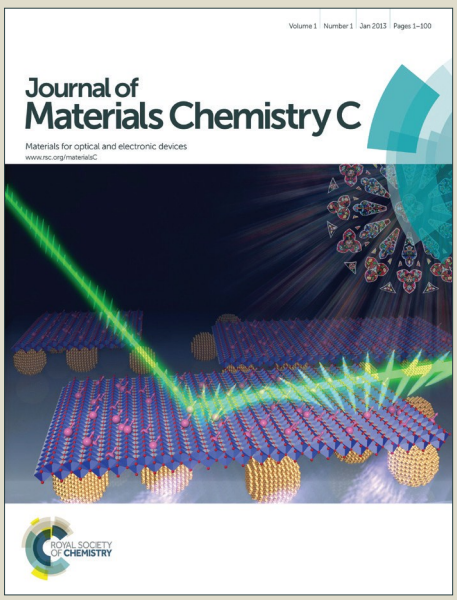

ROYAL SOCIETY OF CHEMISTRY

www.rsc.org/materialsC

Journal of Materials Chemistry C RSCPublishing

ARTICLE

Energy level tuning of blue emitting and electron transporting vinylene bis(vinyl quinolinyl) benzene derivatives: synthesis, characterisation, thin film characterisation and performance in OLEDs

Cite this: DOI: 10.1039/xoxxoooooox

Received ooth January 2012,
Accepted ooth January 2012

DOI: 10.1039/xoxxoooooox

www.rsc.org/

Poopathy Kathirgamanathan *[a], Sivagnanasundram Surendrakumar[a], Seenivasagam Ravichandran[a], Muttulingam Kumaraverl[a], Juan Antipan Lara[a], Subramaniam Ganeshamurugan[a], Lisa M. Bushby[a], Jeremiah P. Tidey[b] and Alexander J. Blake*[b]

A number of thermally stable, conjugated, blue emitting vinylene bis(vinyl quinolinyl)benzene derivatives were prepared and three of them were characterised by singly crystal X-ray crystallography. They exhibit blue to blueish green emission (fluoresecence and electroluminescence) depending on the substituents. Their effectiveness as electron transporters in red and green organic light emitting diodes (OLEDs) has been explored. The phenyl and naphthyl substituted compounds were found to be superior to Alq_3 in OLEDs as electron transporters. The electron mobility of the parent molecule, phenyl, thienyl and naphthyl substituted compounds were determined to be 8 x 10^{-7}, 3.3 x 10^{-6}, 5.5 x 10^{-6} and 8 x 10^{-6}
cm^2 V^{-1} s^{-1} respectively. Lifetime measurements were carried out for the red and green fluorescent devices and compared with Alq_3 as an electron transporter. Some vinylene bis(vinyl quinolinyl) benzene derivatives show significantly longer lifetimes than analogous devices made with Alq_3 as the electron transport layer.
Purple to dark blue emitting devices were achieved from two of the derivatives.

1. Introduction

Manipulating the electronic, optical and thermal properties of organic semiconductors is a major area of research as they find widespread applicability[1-7, 13-18]. Over the last five years organic light emitting diodes (OLEDs) have evolved into a mature technology and flexible OLEDs are also under development[1].

Displays based on organic light emitting diodes (OLEDs) have become one of the significant flat panel display technologies, as evidenced by the production of active matrix OLEDs for mobile phones by Samsung SDI and the introduction of 56" OLED-TVs by Samsung and LG Displays (Korea). However, high performance organic semiconductors are still required to improve the performance of these devices.

It is well known that the HOMO-LUMO levels of the organic semiconductors play a major role in the performance of OLED devices and thus we wanted to probe the band gap tuning with a system such as oligophenylvinylene which permits a large range of synthetic variations. Furthermore, the quinolinoyl moiety is both electron transporting and fluorescent. This paper investigates both properties.

Long operational lifetimes and high electroluminescent efficiencies are very important to commercial success. OLEDs are multilayer devices, typically composed of (i) a hole injector [e.g. copper phthalocyanine (CuPc), 4,4',4"-tris[N-(2-naphthyl)-N-phenyl-amino)triphenylamine (2-TNATA), tripyrazinocyclohexane(s)[1-3]], (ii) a hole transporter [e.g., N,N'-bis-(1-naphthalenyl)-N,N'-bis-phenyl(1,1'-biphenyl)-4,4'-diamine, (α-NPB)], (iii) an emissive layer (host + dopant), (iv) an electron transporter [e.g. tris(8-hydroxyquinoline)aluminium (Alq_3)], (v) an electron injector (e.g., LiF, CsF, lithium quinolates) and (vi) a cathode (e.g. Al)[4-6] to provide charge balance so that efficient devices can be produced. Hole transporters and electron transporters can also be doped with an acceptor or donor, respectively, to increase the conductivities of the respective layers[5-6, 12-29]

There is a continuing demand for reduction of the power consumption and operating voltage of OLEDs and for a lengthening of their lifetime. Charge transport (hole and electron) materials, whether pure or doped, are an integral part of any OLED. It has been reported that nearly 60% of the total electrical power loss in OLEDs is due to the transport layers (hole injecting layer, 5.1 %; hole transporting layer, 7.7 %; hole blocking layer, 5.8 %; electron transporting layer, 35.9 % and electron injecting layer, 5.7 %) for a phosphorescent green device. The remainder is due to the emissive layer (39.8%)[9]. The lifetime is also critically dependent on the nature of the

transporters employed. Improvements in efficiencies of up to 70% have been reported by Kathirgamanathan *et al*[1] and Kido *et al*[8] when Alq_3, is replaced by some novel electron transporters in otherwise identical devices.

A good electron transporter (et) should have the following characteristics[10-13]: (i) high electron affinity to match with the work function (W.F.) of the cathode, thus reducing the energy barrier; (ii) high electron mobility (μ_e > 1 x 10^{-5} cm^2 V^{-1} S^{-1}) to aid the transport of electrons into the emissive layer and efficiently confine the excitons in this layer; (iii) a reversible electrochemical reduction with a sufficiently high reduction potential; (iv) a high ionisation potential (I.P.) to serve as a hole blocker (I.P. > 6 e.V.); (v) a high glass transition temperature and melting point; (vi) thermal stability up to at least 250°C (high $T_g/T_m/T_d$); (vii) stability under evaporation conditions for a period of at least 144 hours if vacuum processing is employed; (viii) good stability to moisture and oxygen; (ix) capable of forming amorphous film so that crystallisation induced degradation is avoided; (x) photostability; (xi) if phosphorescent emitters are used, the triplet energy level of the et should be higher than that of the phosphorescent emitters; (xii) processability to produce uniform and pinhole-free films either by evaporation (small molecules) or by solution casting.

A variety of ets based on metal quinolinolate(s) (e.g. Alq_3, Inq_3, Gaq_3, Scq_3, Mgq_2), oxadiazole(s), imidazole(s), pyridine derivatives, perfluorinated oligophenylene(s), silole(s), phenanthroline(s), boron compounds and pyrimidone(s) have been reported[7, 8]. However, despite its low electron mobility and instability to holes, Alq_3 has remained the material of choice due to its low cost and acceptable OLED lifetimes. Alq_3 has three major drawbacks: (i) it leaves behind a considerable amount of residue during sublimation purification and OLED production conditions: (ii) the operating voltage is still relatively high and (iii) there is a perceived toxicity of aluminium compounds.

We have been interested in charge transporting materials for OLEDs over the last 20 years. Metal complexes leave behind residues on evaporation under manufacturing conditions. Thus, non-metal-based electron transporters which could potentially leave no residue under vacuum thermal evaporation conditions are of immense value to OLED manufacturers. This paper reports our successful attempt in synthesising organic electron transporters.

Here we report the synthesis and application of bis(vinyl quinolinyl) benzene derivatives as non-metal based alternative electron transporters superior in performance to the "workhorse" Alq_3. We also report energy level tuning by substituting the bis (vinyl quinolinyl) benzene (hereafter called E278-ST) with phenyl (E278-Ph-ST), thienyl (E278-Th-ST), naphthyl (E278-Np-ST) and pyrenyl (E278-Pyr-ST). The substituted quinolinyl derivatives were synthesised by Suzuki-Miyaura coupling as illustrated in Scheme 1.

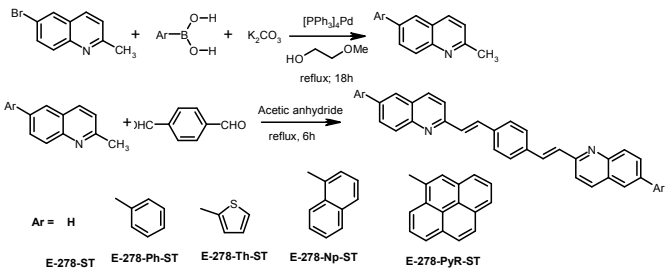

Scheme 1. Synthesis of selected bis(vinyl quinolinyl) benzene derivatives

2. Experimental

Device fabrication

Electron-only devices were fabricated by evaporating E278-ST and a selected number of its derivatives of layer thickness of 50 to 120 nm into a ITO/LiF/E278-X/LiF/Al device structure. Alq_3 devices were also made for comparison. Hole-only devices were also fabricated as ITO/MoO_3/E278-X/MoO_3/Al using E278-ST, E278-Ph-ST and α-NPB (for comparison).

Detailed electroluminescent characteristics were carried out only on E278-ST, E278-Ph-ST and E278-Th-ST since we had crystal structures for them only. The device structure was ITO (anode)/E278-X (50 nm)/LiF (1 nm)/Al (cathode).

Trilayer devices were also fabricated in order to establish the electron transporting characteristics of E-278-X the devices. The device structure was ITO/ZnTpTP(HIL)/α-NPB (HTL)/E-278-X /LiF/Al.

Electroluminescent devices were fabricated by vacuum thermal evaporation method using a multi-chamber OLED pilot machine (Solciet OLED System, purchased from ULVAC, Japan). The devices were fabricated on a patterned (pixelated ITO substrate 40 ohms per square, surface resistance); Hitachi High Tech., Japan), cleaned with water, acetone, isopropyl alcohol and water (in that order), dried at 150 °C for 20 minutes and then subjected to ozone cleaning (UV irradiation, 185 nm) at 150 °C for 10 minutes. The substrate was then plasma-cleaned in the presence of oxygen for 25 seconds and moved into the vacuum chamber from which the hole injector [(5,10, 15, 20-tetra(p-tolyl)-21H, 23H-porphine)zinc(II)] (ZnTpTP), 20 nm for red devices and 50 nm for green devices, hole transporter [N,N'-bis-(1-naphthalenyl)-N,N'-bis-phenyl-(1,1'-biphenyl)-4,4'-diamine, (α-NPB), 50 nm], host: dopant [Alq_3, (50 nm): (0.1 nm) dopant (N,N'-diphenylquinacridone (DPQA), co-evaporation], electron transporter [either Alq_3 or Zrq_4 (20 nm)] E-278-X were sequentially deposited. The evaporation rates of ZnTpTP, α-NPB, (Alq_3, DPQA), E278-X and LiF (electron injector) were 1 Å/s, 1.6 Å/s, (1 Å/s, 0.1 Å/s), 1 Å/s and 0.05 Å/s respectively.

Directly from the vacuum chamber, all the devices were encapsulated using UV curable adhesive (Nagase) with glass back plates in a glove box filled with dry nitrogen so that the devices were not exposed to air. The electrical and optical measurements were carried out by a computer-controlled Keithley 2400 Source Meter and a Minolta (CS-1000) spectrometer, respectively. HOMO-LUMO levels were determined by cyclic voltammetry (by computer-controlled potentiostat PAR 273 or CHI 600D) and from band gap measurements by absorption spectroscopy of thin films produced by vacuum thermal evaporation. Capacitance measurements were made on thin films as well as compacted discs using an impedance analyser (Hewlett Packard, 4284A). DC conductivity measurements of the materials were also performed on compacted discs using a two-probe method[24].

3. Results and Discussion

3.1 Physical properties

The band gap of the E278-ST derivatives under investigation was determined from the absorption edge of thin films

produced by vacuum thermal evaporation (Fig. 1). It is immediately apparent that phenyl and thienyl substituents lower the band gap while napthyl and pyrenyl substituents increase the band gap. Due to the increased conjugation, the band gap of the fused ring system is expected to decrease, but contrary to expectation, the band gap of the fused ring substitution increases with increasing conjugation. We believe that this is due to non-planarity of the molecules, E278-Np-ST and E278-PyR-ST which twists the quinolinyl moiety, thus increasing the band gap.

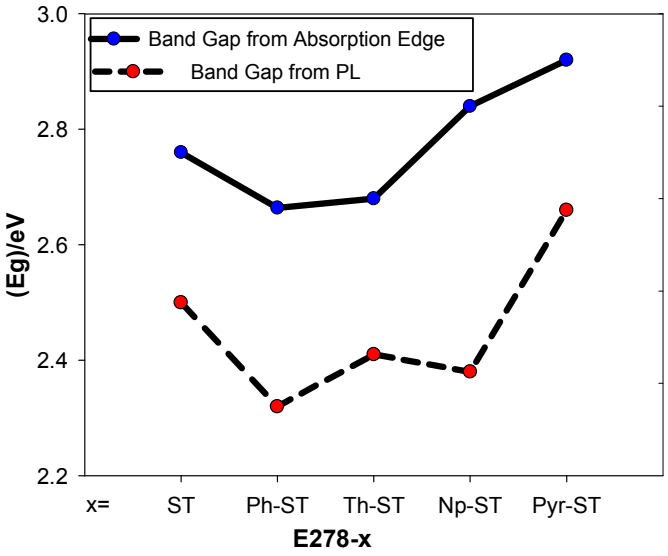

Figure 1 Comparison of band gaps from absorption edge of photoluminescence

3.2 Crystal structure analysis

Crystals of E278-ST, E278-Ph-ST and E278-Th-ST suitable for single-crystal X-ray crystallographic studies were grown by slow vacuum sublimation at a temperature of 300 °C and a pressure of 5 x 10^{-6} Torr. The tube furnace where the compounds were sublimed crystallised had a gradient of three different temperature zones. The temperature of the material containing bulb of the tube was gradually increased and kept at 300 °C. The crystals were obtained at the temperature zone of 250 °C.

Diffraction data were collected at 120(2) K on Agilent Technologies SuperNova diffractometers equipped with microfocus copper X-ray sources, mirror optics and Atlas or Eos CCD detectors. Data collection and processing utilised CrysAlisPRO[34] The structures were solved by direct methods[35] and refined using full-matrix least squares[36, 37]. Rotation disorder in the thiophene rings was modelled with the use of similarity and planarity restraints to the relevant geometric parameters; restraints were also applied to the displacement parameters of the thiophene ring; the occupancy of the major component refined to 0.8426(9). Crystal structure diagrams were produced using MERCURY[38] and other material was produced for publication using OLEX2[37]. CCDC 1044135−1044137 contain the supplementary crystallographic data for this paper in CIF format. These data can be obtained free of charge from The Cambridge Crystallographic Data Centre via *www.ccdc.cam.ac.uk/data_request/cif*.

The asymmetric unit of E278-ST comprises two half-molecules disposed about crystallographic inversion centres. The two molecules differ in their degree of planarity: one is planar to within 0.031 Å, while the other is only planar to within 0.197 Å and exhibits a marked sinusoidal shape. This is also illustrated by the dihedral angles: while those between the fused rings of the quinolinyl group [1.19(13), 1.16(13) °] are equivalent in the two molecules, the angles between the quinolinyl groups and the central phenyl rings [1.95(13), 12.80(13) °] differ markedly.

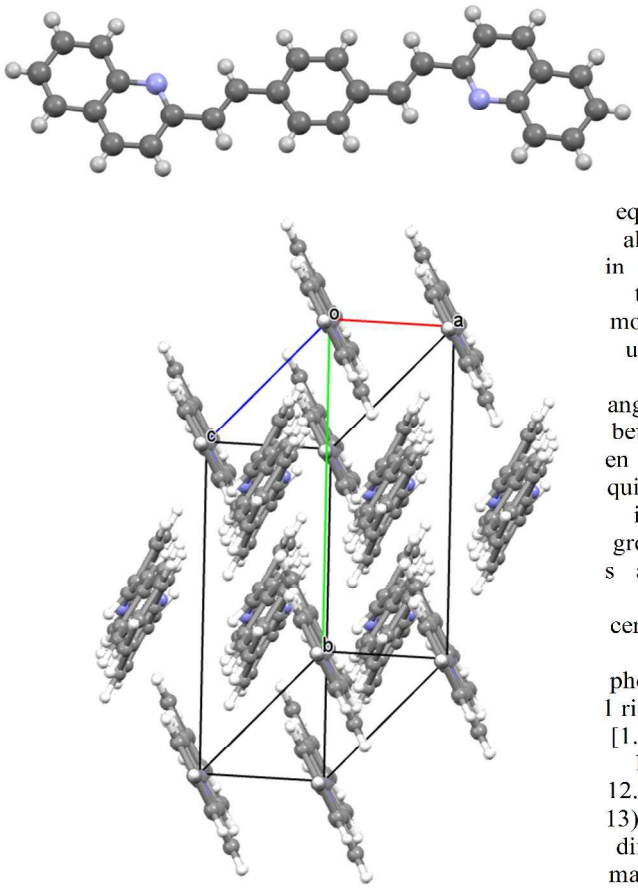

Molecules of E278-ST pack in a herringbone arrangement (Figure 2) as the result of CH…π, π…π and CH…N interactions.

Figure 2 Upper, view of a single molecule of E278-ST; lower, packing of molecules of E278-ST. N atoms are shaded blue, C black and H light grey

In E278-Ph-ST, the asymmetric unit comprises a half-molecule, the other half of which is generated by the operation of an inversion centre. The dihedral angle between the fused rings of the quinolinyl group [1.91(7) °] is somewhat greater than in E278-ST; that between the quinolinyl group and the central phenyl ring [12.19(7) °] is similar to the value in one of the molecules of E278-ST. However, a significant deviation from planarity arises from the twist of the terminal phenyl ring relative to the quinolinyl group, where the mean torsion angle is 24.30(7) °. Packing in E278-Ph-ST (Figure 3) also involves a herringbone motif but this comprises C−H…π interactions

only: the twisting of the terminal phenyl ring allows it to form one of the most favourable of these interactions.

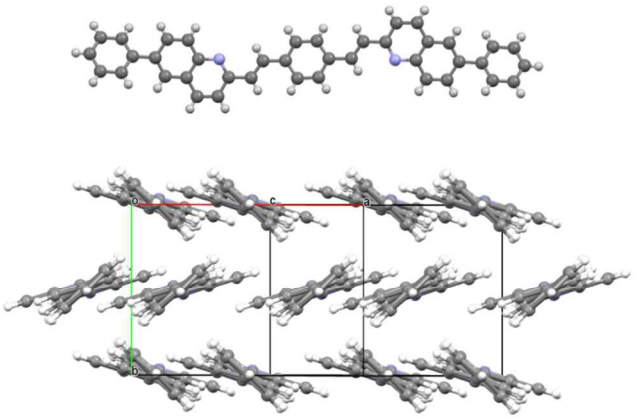

Figure 3 Upper, view of a single molecule of E278-Ph-ST; lower, packing of molecules of E278-Ph-ST. N atoms are shaded blue, C black and H light grey

Molecules of E278-Th-ST have no crystallographically imposed symmetry and are planar to within 0.168 Å. The thiophene rings are both disordered by a rotation of ca. 180 ° about the bonds to their respective quinolinyl groups: the major/minor occupancies are 0.8426(9)/0.1574(9) and 0.8491(9)/0.1509(9). The dihedral angles of 7.57(8) ° and 8.01(8) ° between the major thiophene components and the linked quinolinyl groups may partly reflect the limitations of the disorder modelling. The dihedral angles between the central phenyl rings and its two flanking quinolinyl groups are 8.01(8) and 11.25(7) °, producing the net effect of a molecule that is more planar than E278-Ph-ST. Packing in E278-Th-ST (Figure 4) takes the form of another herringbone motif involving C−H…π interactions.

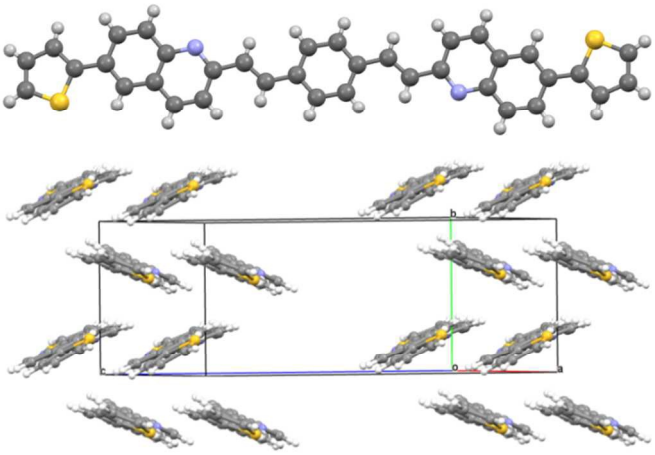

Figure 4 Upper, view of a single molecule of E278-Th-ST; lower, packing of molecules of E278-Th-ST. S atoms are shaded yellow, N blue, C black and H light grey. Only the major component is shown for each disordered thiophene ring

3.3 Thermal characterisation

Differential Scanning Calorimetry (DSC). DSC was carried out on E278-ST, E278-Ph-ST, E278-Th-ST, E278-Np-ST and E278-PyR-ST. DSC of the E278-ST derivatives (Fig. 5, also see Table 1) show higher melting points than that of the parent compound (E278-ST, 246 °C). The melting point follows the order E278-ST < E278-Pyr-ST < E278-Np-ST < E278-Ph-ST < E278-Th-ST. The increase in the melting point is expected as aromatic side groups and fused ring systems enhance the rigidity of a molecule and thus increases the energy required to melt a material. Further, the higher melting point of E278-Th-ST (330 °C) compared to E278-Ph-ST (312 °C) could be explained on the basis that the former is a planar molecule and the latter is not (the phenyl substituent is out of plane) as reducing the efficiency of the packing of the crystal structure (refer to Figure 3).

Only E278-Np-ST and E278-Pyr-ST showed glass transition temperatures (of 94 °C and 88 °C, respectively) and we indeed found them to sublime to produce amorphous

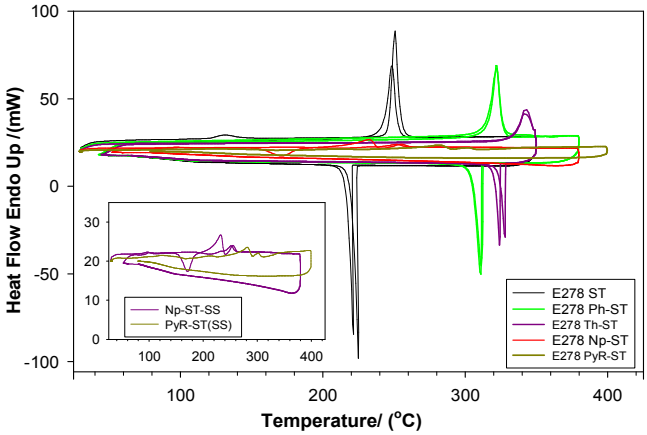

powders whereas E278-ST, E278-Ph-ST and E278-Th-ST all formed crystals on slow sublimation.

Figure 5 Differential scanning calorimetry of E278-ST, E278-Ph-ST, E278-Th-ST, E278-Np-ST and E278-PyR-ST; inset shows the T_g of E278-Np-ST and E278-PyR-ST

Thermogravimetric analysis (TGA). TGA (Fig. 6) under nitrogen shows that all the compounds are stable in air in excess of 300 °C. E278-Ph-ST, E278-Np-ST, E278-Pyr-ST and E278-Th-ST are stable up to 400 °C and E278-Th-ST is remarkably stable up to 499 °C (weight loss of only 2.5 %). It is important that E278-ST and E278-Ph-ST do not leave behind any residues. The compounds are also stable under multiple

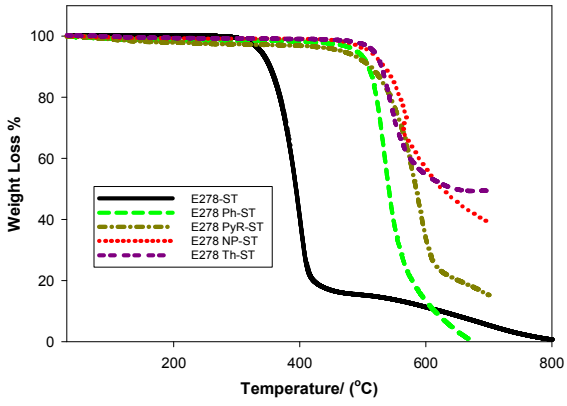

sublimation purification.

Figure 6 Thermogravimetric analysis of E278-ST, E278-Ph-ST, E278-PyR-ST, E278-Np-ST and E278-Th-ST

Table 1 Physical properties of E278-ST and its derivatives

Compound	STRUCTURE	M.P. (DSC) ONSET /°C	T_g /°C	TGA / % wt loss	Band gap /eV
E278-ST	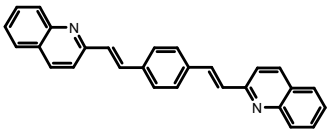	246	-	400 (0%)	2.70
E278-Ph-ST	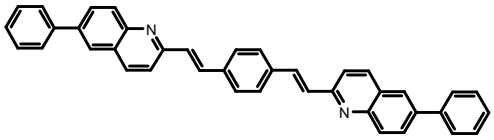	312	-	400 (0%)	2.58
E278-Th-ST	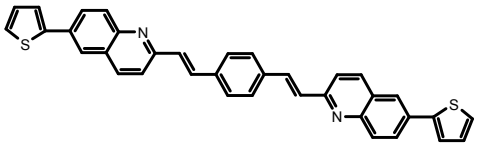	330	-	499 (2.5%)	2.59
E278-Np-ST	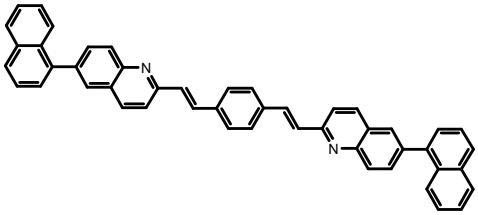	276	94	400 (0.5%)	2.79
E278-PyR-ST	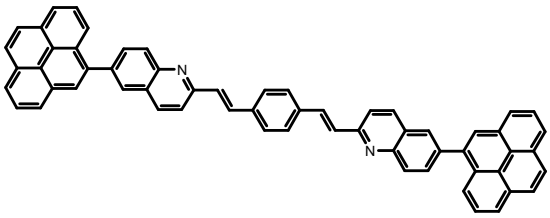	266	88	400 (3%)	2.88

3.4. Optical measurements

Absorption and fluorescence spectroscopy in solution. The derivatives of E278-ST, namely E278-Ph-ST, E278-Th-ST, E278-Np-ST and E278-Pyr-ST, were all found to be fluorescent both in solution and as thin films produced by vacuum thermal evaporation (VTE). Fig. 7 shows the photoluminescent characteristics of the bis(vinyl quinolinyl) benzene derivatives under exposure to UV light. Absorption and fluorescence spectroscopy were carried out in chloroform (Fig. 8).

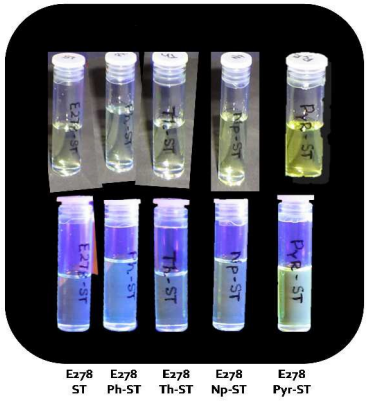

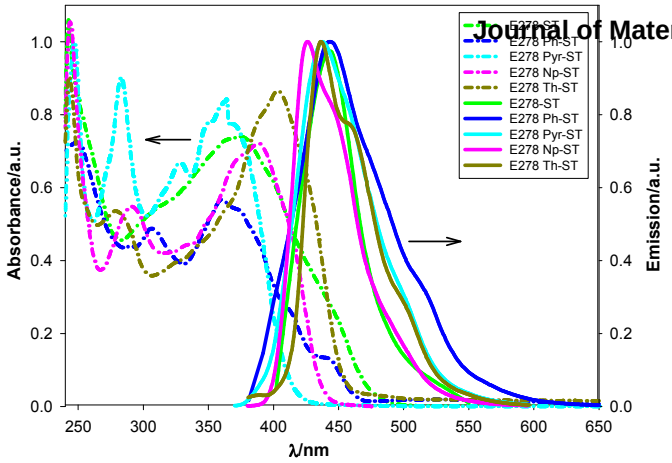

Figure 7 Emission of E278-ST and its derivatives in CHCl3 under normal lighting conditions (top) and upon exposure to UV radiation (bottom)

Figure 8 Absorption and emission spectra of E278-ST (parent) and its derivatives in chloroform

Thin film absorption and fluorescence. UV-Vis absorption and fluorescence spectroscopy was carried out on thin films (thickness approximately 100 nm) produced by vacuum thermal evaporation (Fig. 9). All the materials were sublimed without decomposition and with no loss of vacuum during evaporation. The results are summarised in Table 2.

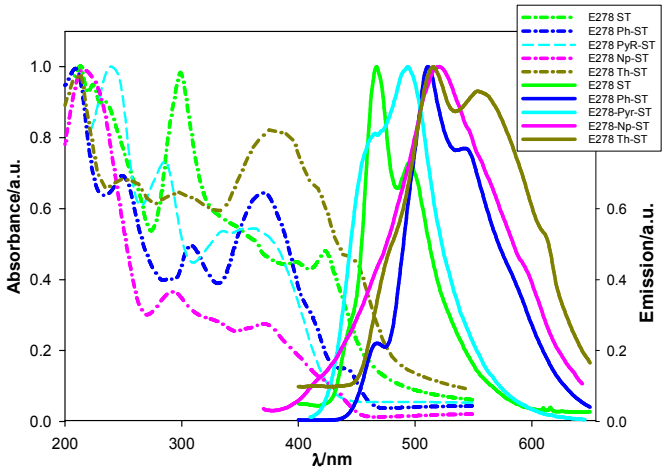

Figure 9 Absorption and emission spectra of the thin film of E278-ST (parent) and its derivatives

The evaporation rate vs temperature plots are shown in Fig. 10. The E278-Pyr-ST has the lowest evaporation temperature required to obtain similar evaporation rate to Alq_3 while all the E278-ST derivatives require higher temperature than Alq_3.

This can be possibly attributed to the large size of the pyrenyl group and the consequent diminished intermolecular interaction.

The photoluminescence (PL) of the thin films (Fig. 9) (where the molecules are constrained) are all red shifted (to longer wavelengths) as expected compared to the PL of the solutions where the molecules are free to move. The red shift ($\lambda_{film} - \lambda_{solution}$) for E278-ST, E278-Ph-ST, E278-Np-ST, E278-PyR-ST and E278-Th-ST are 16, 105, 91, 56 and 63 nm respectively. *We attribute these differences in the PL peak positions as arising primarily from the substituents effects as the peak position of the* of the thin films were largely invariant of the thickness of the film.

Table 2 E278 series: absorption and fluorescence

Compound	Absorption peak λ_{max} / nm in $CHCl_3$ solution (extinction coefficient)	Fluorescence peak λ_{max} / nm in $CHCl_3$ solution	Absorption peak λmax / nm thin film	Fluorescence peak λmax / nm thin film
E278-ST	379 (4.90×10^4)	439	302, 418(sh)	455, 485(sh)
E278-Ph-ST	393 (1.00×10^4)	429	372, 442(sh)	511, 541(sh)
E278-Th-ST	403 (3.90×10^3)	437, 460(sh)	378	511, 555(sh)
E278-Np-ST	388 (4.00×10^4)	430	364	521
E278-PyR-ST	364 (6.98×10^4)	438	363	466(sh), 494

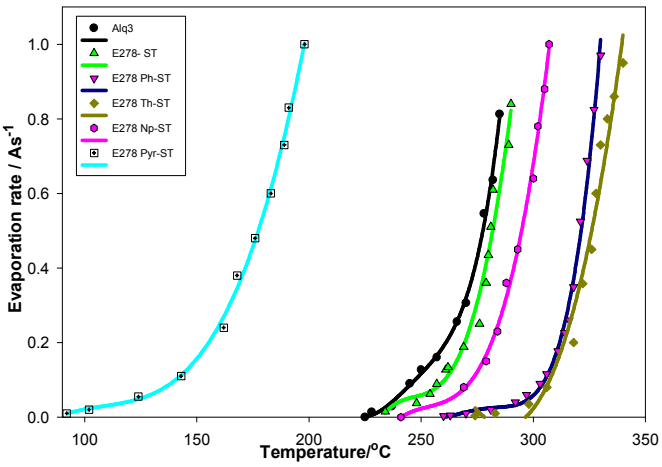

Figure 10 Evaporation rate of E278-ST, E278-Ph-ST, E278-Th-ST, E278-Np-ST and E278-PyR-ST compared to the evaporation rate of Alq_3

3.5. Electrochemical properties

Cyclic voltammetry was performed in dichloromethane containing the analyte E278-ST (0.01 mM), E278-Ph-ST (0.5 mM), E278-Th-ST (0.1 mM) or E278-Np-ST (0.1 mM) except for E278-Ph-ST whose CV was also carried out in acetonitrile because of its poor solubility in dichloromethane (Fig. 12). E278-Pyr-ST was so insoluble in most organic solvents suitable for electrochemistry, that its CV could not be performed.

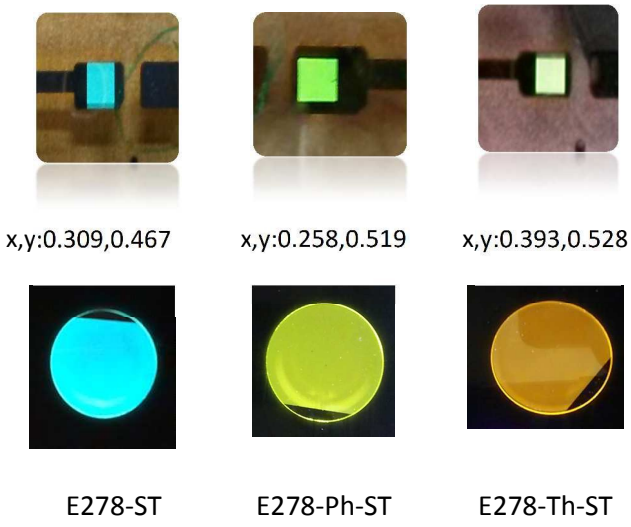

Figure 11 Single layer electroluminescent devices of E278-ST, E278-Ph-ST, E278-Th-ST (top), CIE x,y colour coordinates and the photoluminescence of thin films under 365 nm irradiation (bottom)

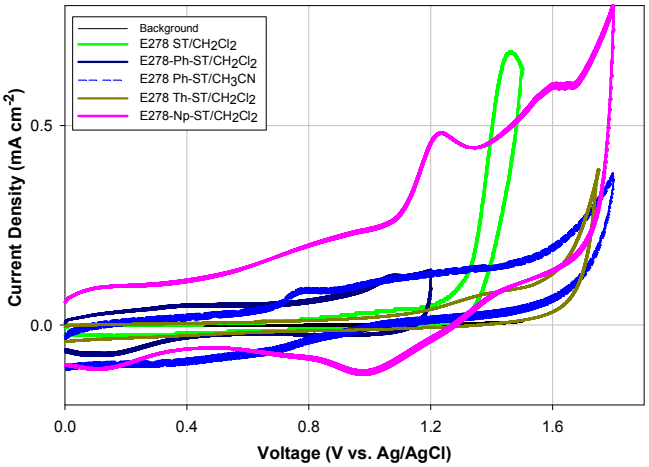

Figure 12 Cyclic voltammetry of E278-ST, E278-Ph-ST, E278-Th-ST and E278-Np-ST in dichloromethane and also E278-Ph-ST in acetonitrile

The supporting electrolyte was tetrabutylammonium hexafluorophosphate (0.2 M) in all case. The working, auxiliary and reference electrodes were Pt (foil), Pt (wire) and Ag/AgCl respectively. The CVs were performed in both the oxidation (0 to 1.8 V) and reduction (0 to -2 V) regions. The CVs were found to be irreversible in both anodic and cathodic scans except for E278-Np-ST which gave quasi-reversible peaks in the anodic scans (Figure 12). Since the cathodic cycles were found to be irreproducible except for E278-ST, we decided to use the anodic scans for the determination of the HOMO levels.

The HOMO levels were determined from the equation in reference[26].

HOMO or LUMO = - ((E1/2 vs. NHE) + 4.40) eV

where NHE = Normal Hydrogen Electrode.

The E1/2 values employed here were determined from the derivative of the cyclic voltammograms. From the absorption band edge of the evaporated thin films, the band gaps of the compounds were deduced and then the LUMO levels were calculated.

The HOMO-LUMO levels of the E278-ST, Ph-ST, Th-ST, Np-ST and PyR-ST are shown in Fig. 13 where they are compared with the HOMO-LUMO of the hole transporter, α-NPB and the electron transporter, Alq_3.

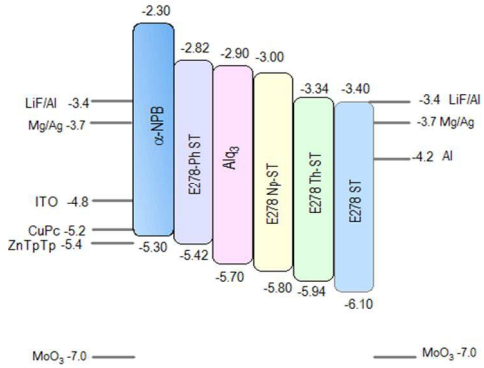

Figure 13 HOMO-LUMO energy levels of E278 series

3.6. Electrical characterisation

Electron-only single layer devices. The electron-only devices (Set A) were fabricated where the anode and the cathode were LiF/Al. Thus, Glass/ITO/LiF /E278-X/LiF/Al where X = ST, Ph-ST, Th-ST. Control devices were also made with Alq_3 (Fig. 14). We also fabricated electron-only devices (Set B), Glass/ITO/Mg, Ag/E278-X/Mg, Ag/Al where X = ST, Ph-ST and Np-ST (Fig. 15). We fitted the current density (J_d) vs. Field (E) to diode, Fowler Nordheim and space charge limited current (SCLC) models[11-12] and found that the data fitted well to the SCLC model, but not to others. The conductivity (DC and AC) and the permittivity of the materials were measured on compacted discs (two probe method) [24]. The conductivity of the complexes was so low (< 1 x 10^{-8} S cm^{-1}) that four probe measurements could not be carried out [19-23]. The data are summarised in Table 3.

Table 3 DC and AC conductivity (100 kHz) and relative permittivity (compacted discs)

Compound	DC conductivity (σ) S cm^{-1}	AC conductivity (σ) S cm^{-1} at 100 kHz	Relative permittivity at 100 kHz ($\varepsilon_r = \varepsilon/\varepsilon_0$
Alq_3	5 x 10^{-13}	5 x 10^{-10}	3.06 ± 0.10
E278-ST	5 x 10^{-13}	5 x 10^{-10}	3.1 ± 0.10
E278-Ph-ST	1 x 10^{-13}	2 x 10^{-10}	3.2 ± 0.10
E278-Th-ST	1 x 10^{-12}	5 x 10^{-10}	3.3 ± 0.10
E278-Np-ST	9 x 10^{-12}	6 x 10^{-9}	3.0 ± 0.10

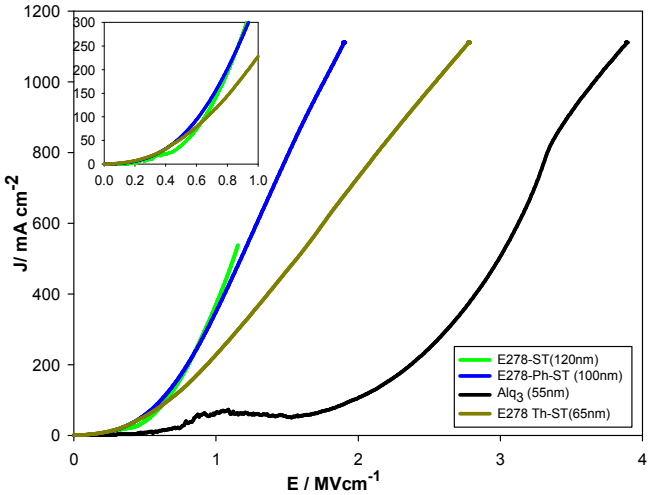

Figure 14 Electron-only devices, current density (mA cm^{-2}) vs field (MV cm^{-1}); Device structure: ITO/LiF (0.5 nm)/E278-X/LiF (0.5 nm)/Al (75 nm)

In the case of Alq_3 based devices, a negative differential resistance (NDR) was observed. This behaviour has been observed by ourselves in a large number of devices whether they were single or multilayer as has been observed by others[39]. The reason for this behaviour could be attributed to a number of factors such as (i). The reduction of Alq3 at the cathode[39c] (ii). Tunnelling effects [39e], (iii). adventitious doping of Alq3 with nitrogen during encapsulation in a nitrogen filled glove box, generating hopping sites (guest hopping sites, GHS)[39d-e].

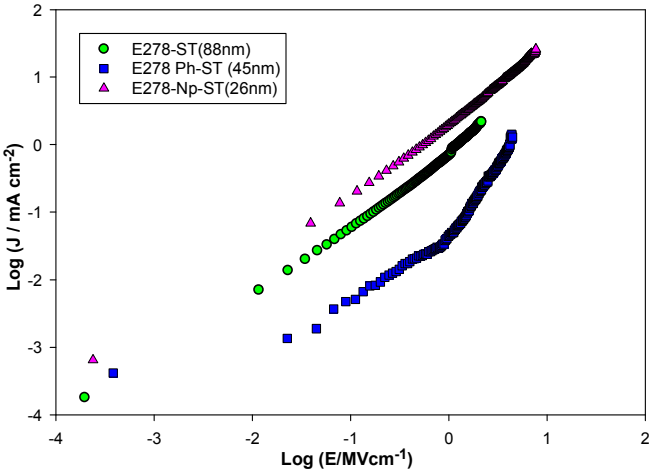

Figure 15 Electron-only devices, current density (mA cm^{-2}) vs field (MV cm^{-1}); Device structure: Glass/ITO/Mg, Ag/E278-X/Mg, Ag/Al

The current density vs. field (Figure 14) for the electron only (Set A) devices, ITO/LiF/E278-ST/LiF/Al show that the electron injection characteristics of E278-Th-ST was found to be best (E278-Th-ST > E278-Ph-ST > E278-ST >>> Alq_3) at low field, but worst at high field (E278-ST > E278-Ph-ST > E278-Th-ST >>> Alq_3) but it is still better than Alq_3. However, the differences are small among the E278 derivatives, but they were all significantly higher than Alq_3.

The devices of ITO/Mg/Ag/E278-X/Mg/Ag/Al (Set B, Figure 15), where X = ST, Ph-ST and Np-ST) show current injection in the following order: E278-Np-ST > E278-ST > E278-Ph-ST at all field strength tested. We observed that ITO/LiF/E278-Np-ST/LiF /Al devices were unstable and irreproducible while E278-Th-ST was not stable with Mg/Ag contact. It should be noted that the reason for the reduction in the magnitude of the current for a given field compared to the ITO/LiF/E278-X/LiF/Al devices is due to the fact that the work function of Mg/Ag (3.7 eV) is higher than that of LiF/Al (3.4 eV).

It can be deduced that the electron injection characteristics should follow the order E278-Np-ST > E278-ST > E278-Ph-ST > E278-Th-ST > Alq_3 at least at medium and high fields employed in OLED devices.

Thin film conductivity was determined from the Ohmic region ($J_d \propto V$) and the mobility was calculated from the space charge region ($J_d \propto V^2$) using the equation[1, 32]

$$J_{SCLC} = (9/8)\, \varepsilon\, \mu\, V^2/d^3$$

where J_{SCLC} = current density in the SCLC region, ε = permittivity, μ = mobility, V = voltage and d = thickness. The data obtained from the hole-only and electron-only devices are summarised in Table 4.

Table 4 Thin film conductivity, electron and hole mobility of Alq_3, E278-ST, E278-Ph_ST, E278-Th-ST and E278-Np-ST

	Thin film conductivity (S cm^{-1}) from electron-only devices	Thin film conductivity (S cm^{-1}) from hole-only devices	Electron mobility (μ_e/cm^2 V^{-1} s^{-1}) from electron-only devices	Hole mobility (μ_h/cm^2 V^{-1} s^{-1}) from hole-only devices
Alq_3	7.5×10^{-10}	4.8×10^{-11}	4.4×10^{-7}	1.1×10^{-8}
E278-ST	5.0×10^{-9}	$1.6 \times ^{-10}$	8×10^{-7}	3×10^{-8}
E278-Ph-ST	4.0×10^{-8}	3.2×10^{-11}	3.3×10^{-6}	1.7×10^{-9}
E278-Th-ST	1.0×10^{-7}	(a)	5.5×10^{-6}	(a)
E278-Np-ST	7.5×10^{-7}	(a)	8×10^{-6}	(a)

(a) not measured due to device instability

Hole-only devices. Hole-only devices (ITO/MoO_3 (10 nm)/E278-X (100 nm)/MoO_3 (10 nm)/Al (100 nm) were fabricated only for E278-ST and E278-Ph-ST (Fig. 16) as the other materials were not stable during measurements. A control device was also made with α-NPB, a well-known hole transporter. We obtained a hole mobility of 1×10^{-5} cm^2 V^{-1} s^{-1} for α-NPB consistent with published data. Table 5 summarises the electron and hole mobilities of E278-ST, E278-Ph-ST,

E278-Th-ST and E278-Np-ST.

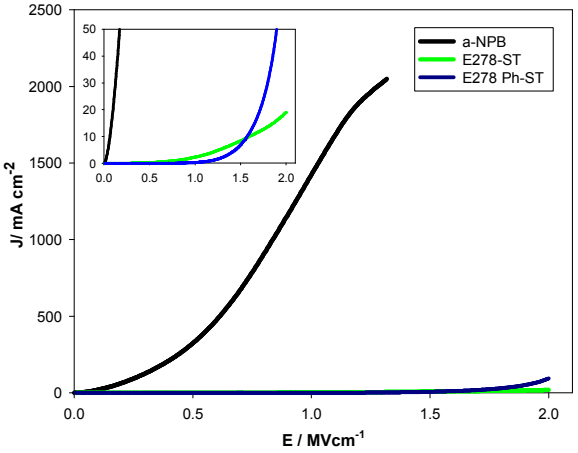

Figure 16 Hole-only devices, current density (mA cm^{-2}) vs field ($MVcm^{-1}$); Device structure: Glass/ITO/MoO_3/E278-X/MoO_3/Al

The hole injection was highest for α-NPB at all the field tested. At low field (E < 1.6 MV cm^{-1}), the hole injection current follow the order: α-NPB > E278-ST > E278-Ph-ST and at high field (E > 1.7 $MVcm^{-1}$), the order was α-NPB > E278-Ph-ST > E278-ST.

Table 5 Comparison of electron and hole mobilities of Alq_3, E278-ST, E278-Ph_ST, E278-Th-ST and E278-Np-ST

	Electron mobility (μ_e/cm^2 V^{-1} s^{-1}) from electron-only devices	Hole mobility (μ_h/cm^2 V^{-1} s^{-1}) from hole-only devices	μ_e/μ_h
Alq_3	4.4 x 10^{-7}	1.1 x 10^{-8}	40.0
E278-ST	8 x 10^{-7}	3 x 10^{-8}	26.7
E278-Ph-ST	3.3 x 10^{-6}	1.7 x 10^{-9}	1941
E278-Th-ST	5.5 x 10^{-6}	a	NA
E278-Np-ST	8 x 10^{-6}	a	NA

(a) not measured due to device instability

It is worth noting that the substitution of the phenyl group and the consequent twisting of the molecule makes the E278-Ph-ST more electron-transporting and less hole-transporting than the parent E278-ST (Table 5). The thin film conductivity measured both under electron only condition and hole only conduction are significantly higher than the corresponding disc conduction (Table 6). This is not surprising as the molecules orient themselves in films as opposed to discs under isotropic compaction. The anisotropic behaviour (Table 6) of the films would affect the device performance as well as the optical properties[19, 33].

Table 6 Degree of Anisotropy

Compound	$\sigma_{electron}$ (thin film only) / σ_{disc}	σ_{hole} (thin film only)/ σ_{disc}
Alq_3	1.5 x 10^3	9.6 x 10^1
E278-ST	1.0 x 10^6	3,2 x 10^2
E278-Ph-ST	4.0 x 10^5	3.2 x 10^2
E278-Th-ST	1.0 x 10^5	Not available
E278-Np-ST	8.33 x 10^4	Not available

3.7. Light emitting devices

Single layer light emitting devices. Single layer devices (ITO/E278-X/LiF/Al) were fabricated to determine the transport properties of the E278-ST, E278-Ph-ST and E278-Th-ST. The current injection (Fig. 17) seems to follow the order E278-ST > E278-Th-ST > E278-Ph-ST although the electron mobilities show E278-Th-ST > E278-Ph-ST > E278-ST, but the differences in mobilities are quite small. We attribute the current injection behaviour in the single layer light emitting devices is entirely
governed by the barrier height on the cathode side[12] which is 0 eV, 0.06 eV and 0.58 eV for E278-ST, E278-Th-St and E278-Ph-ST respectively.

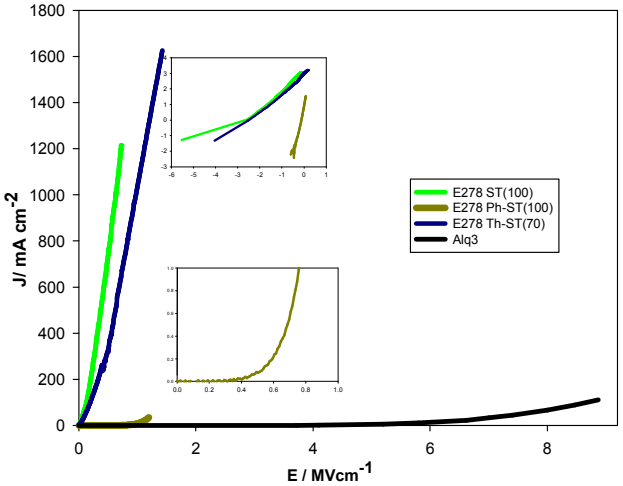

Figure 17 Single layer EL devices (ITO/E278-X/LiF/Al; where X= ST, Ph-ST and Th-ST)

The devices were of poor efficiency and the maximum luminance achieved was 21 cd m^{-2}. This is attributed to the poor hole injection into E278-X as no hole injector or transporter was used. However, it is worth noting that the E278-X/LiF/Al interface is more effective than Alq3/LiF/Al in terms current injection. Further, the free Li formed at the LiF/Al interface has no detrimental effect on the E278-X systems[2b].

Electroluminescent characteristics of ITO/E278-X/LiF/Al. The electroluminescent characteristics of the single layer devices

	Cathode side barrier /eV	Anode side barrier /eV	Turn on voltage (V_t/V) (a)	Current efficiency /cdA^{-1} (b)	Power eff W
E278-ST	0.00	1.3	3.0 ± 0.2	1 x 10^{-1}	2 x
E278-Ph-ST	0.58	0.62	6.0 ± 0.2	3.6 x 10^{-2}	1.6 x
E278-Th-ST	0.06	1.14	3.5 ± 0.2	2.7 x 10^{-3}	2 x 10^{-3}

Table 7 Electroluminescent performances of the single layer devices for E278-ST, E278-Ph-ST and E278-Th-ST (a) at 1 cdm^{-2}; (b) at 10 cdm^{-2}

are summarised in Table 7. The performance of the single layer electroluminescent devices was poor owing to the lack of hole injection and consequent charge injection imbalance. Electroluminescence requires the injection of both holes and electrons and this is determined by the barrier heights of the anodic and cathodic sides. It should be mentioned that E278-ST and E278-Th-ST are planar molecules while E278-Ph-ST is not (as shown by the crystal structure, see Fig. 3). The turn-on voltage follows the barrier presented to the device on both anode and the cathode side.

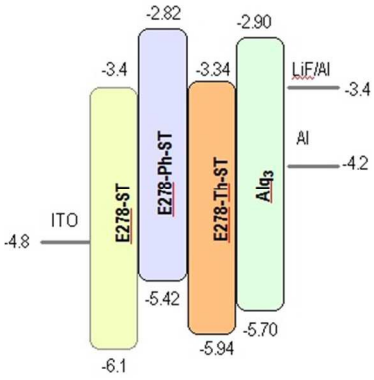

Figure 18 Energy level diagram of single layer device (ITO/E278-X/LiF/Al)

The EL spectra of E278-Ph-ST and E278-Th-ST were almost identical to their respective PL spectra indicating that the same excited state is involved whereas the EL spectrum of E278-ST is substantially red-shifted compared to its PL and featureless. We have established that there is no decomposition on evaporation of E278-ST by taking samples from the evaporated thin films and carrying out elemental analysis and crystal structure where we obtained identical chemical composition. Thus, we conclude that the red shift is due to the effect of orientation of the molecule on the ITO and hence the excited state is different of the E278-X derivatives (Fig 19). The difference in the orientation[33] could result from the evaporation rates employed in the device manufacture (1 Å s^{-1}) as opposed to the thin film for PL produced in excess of 50 Å s^{-1}.

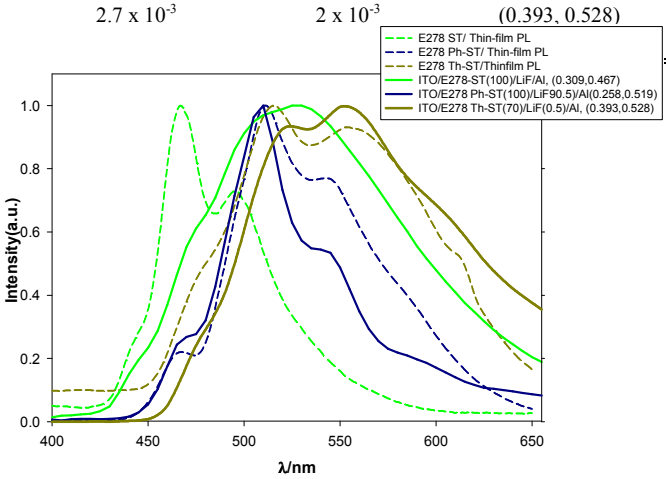

Figure 19 Comparison of the electroluminescent (EL) and photoluminescent (PL) spectra of the single layer devices of E278-ST, E278-Ph-ST and E278-Np-ST; Device Structure: ITO/E278-X (100 nm)/LiF/Al

Figure 20 Energy diagram of tri-layer device, ITO/ZnTpTP (10 nm)/α-NPB (50 nm)/E278-X (50 nm)/LiF (0.5 nm)/Al

E278-X as an electron transporter in tri-layer electroluminescent devices.

In order to increase the hole injection, we fabricated tri-layer devices composed of a hole injecting layer and a hole transporting layer. The hole injector ZnTpTP and the hole transporter α-NPB were employed to enhance the hole injection into the emissive layer; ITO/ZnTpTP (10 nm)/α-NPB (50 nm)/E278-X (50 nm)/LiF (0.5 nm)/Al where the E278-ST, E278-Ph-ST and E278-Th-ST act as both emissive and electron transporting layer. The hole injector ZnTpTP was used to enhance the hole injection and to planarize the ITO surface. α-NPB acts as the hole transporter. Their performances are summarised in Table 8.

	Barrier height with α-NPB /eV	Cathode side barrier height /eV	Turn on voltage (V_t)/V (a)	Current efficiency /cdA^{-1} (b)	Power efficiency /lm W^{-1} (b)	1931-Colour coordinates CIE (x, y)
E278-ST	0.80	0.00	4.5 ± 0.1	2.5 x 10^{-1}	1.0 x 10^{-1}	(0.351, 0.505)
E278-Ph-ST	0.12	0.58	3.7 ± 0.1	6.0 x 10^{-1}	2.7 x 10^{-1}	(0.370, 0.546)
E278-Th-ST	0.64	0.06	5.2 ± 0.1	3.5 x 10^{-1}	1.2 x 10^{-1}	(0.362, 0.517)

Table 8 Electroluminescent performances of the three layer devices of ITO/ZnTpTP (10 nm)/α-NPB (50 nm)/E278-X (50 nm)/LiF (0.5 nm)/Al; where E278-X = E278-ST, E278-Ph-ST and E278-Th-ST

As in the case of single layer devices (namely, ITO/E278-X/LiF/Al), the EL spectra of E278-ST is significantly different from its thin film PL indicating that different excited states are involved in the PL and EL. However, as in the case of single layer devices, the EL and PL of the E278-Ph-ST and E278-Th-ST are virtually identical indicating that the same excited states are involved (Fig 21).

As expected[14-15], the introduction of the hole transport layer improves the current efficiency of E278-ST, E278-Ph-ST, E278-Th-ST by 2.5, 17 and 130 fold.

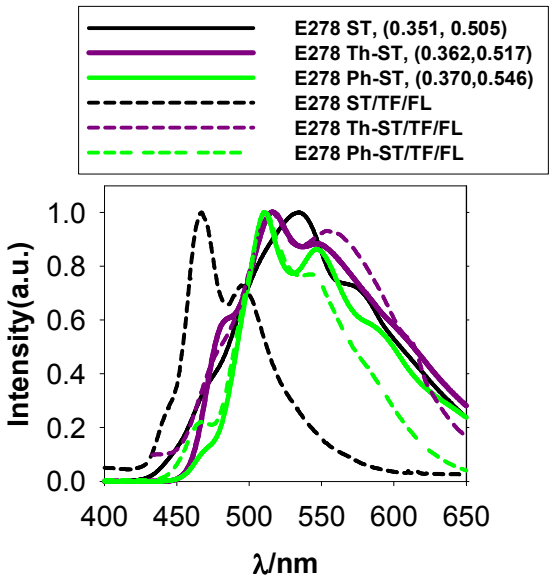

Figure 21 Comparison of the electroluminescent (EL) and photoluminescent (PL) spectra of the three layer devices; Device structure: ITO/ZnTpTP (10 nm)/α-NPB (50 nm)/E278-X (50 nm)/LiF (0.5 nm)/Al

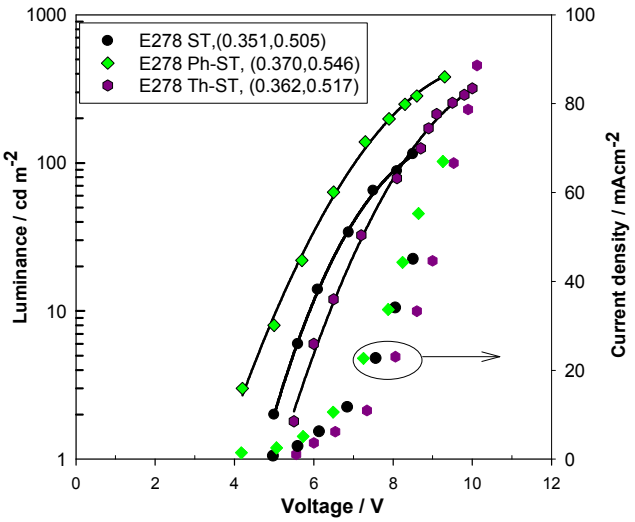

Figure 22 Luminance and current density (J) vs voltage plots of the devices: ITO/ZnTpTP (10 nm)/α-NPB (50 nm)/E278-X (50 nm)/LiF (0.5 nm)/Al

The current density vs voltage plot (Figure 22) shows that the current injection is highest for E278-Ph-ST and then E278-ST and E278-Th-ST in that order (i.e. E278-Ph-ST > E278-ST > E278-Th-ST). The maximum luminance levels achieved for the tri layer devices are around 400 cdm^{-2} as a result of increased hole injection compared to the single layer devices for which the maximum luminance achieved was only 20 cd m^{-2}.

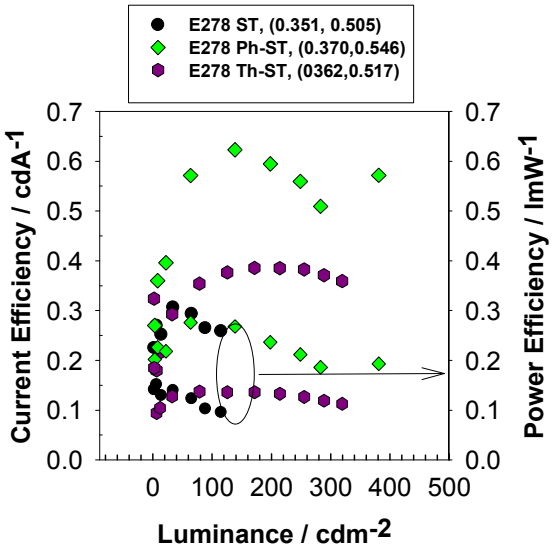

Figure 23 Current efficiency vs luminance and power efficiency vs luminance plot of the devices: ITO/ZnTpTP (10 nm)/α-NPB (50 nm)/E278-X (50 nm)/LiF (0.5 nm)/Al

Electron transporting characteristics of E278-X in red devices

Red devices were fabricated using Alq_3 and rubrene as co-host and 4-(dicyanomethylene)-2-i-propyl-6-(1, 1, 7, 7-tetramethyljulolidyl-9-enyl)-4H-pyran (DCJTI) as the red fluorescent emitter. The device performance of the red devices (ITO/ZnTpTP (20 nm)/α-NPB (60 nm)/Alq_3: Rub: DCJTI (30:30:0.7 nm)/ETL (30 nm)/LiF (0.5 nm)/Al) are shown in Fig. (25-28) and summarised in Table 9.

The efficiency improvement by both E278-Ph-ST and E278-Naph-ST over Alq_3 as etl is attributed mainly to their higher electron mobility than Alq_3. E278-Naph-ST has slightly deeper HOMO level than the host Alq_3, but the current efficiency between the E278-Ph-ST and that of E278-Naph-ST is not significant, but E278-Naph-ST gives higher power efficiency.

We believe that the main mechanism is enhanced electron injection rather than any hole blocking property of E278-Naph-ST.

Table 9 Performance data for the red devices. Device structure: ITO/ZnTpTP (20 nm)/α-NPB (60 nm)/Alq_3: Rub: DCJTI (30:30:0.7 nm)/ETL (30 nm)/LiF (0.5 nm)/Al

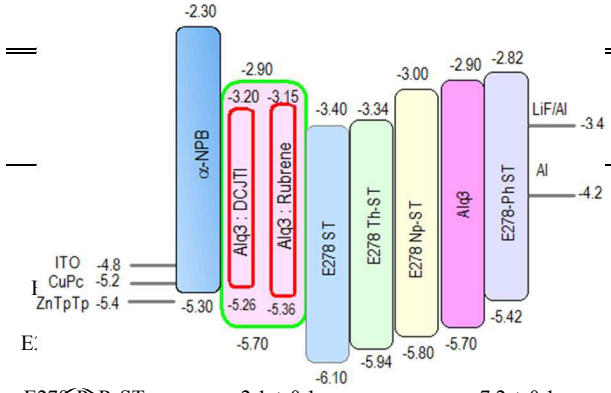

	CIE (x, y) (b)	Current efficiency η /cd A^{-1} (b)	Power efficiency η /lm W^{-1} (b)
TI Rubrene	(0.652, 0.347)	4.0 ± 0.1	1.5 ± 0.1
	(0.647, 0.353)	3.2 ± 0.1	1.2 ± 0.1
	(0.651, 0.349)	4.5 ± 0.1	2.2 ± 0.1
E	(0.650, 0.350)	4.6 ± 0.1	1.8 ± 0.1
E278-PyR-ST	2.1 ± 0.1	7.2 ± 0.1	(0.659, 0.341) 3.5 ± 0.1 1.5 ± 0.1

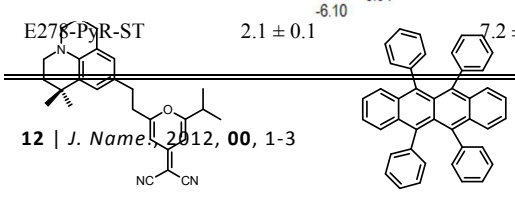

Figure 24 Energy level diagram for device structure: ITO/ZnTpTP (20 nm)/α-NPB (60 nm)/Alq_3: Rub: DCJTI (30:30:0.7 nm)/ETL (30 nm)/LiF (0.5 nm)/Al

Figure 25 Current density (linear and log) and luminance vs voltage plots for the red device ITO/ZnTpTP (20 nm)/α-NPB (60 nm)/Alq_3: Rub: DCJTI (30:30:0.7 nm)/ETL (30 nm)/LiF (0.5 nm)/Al

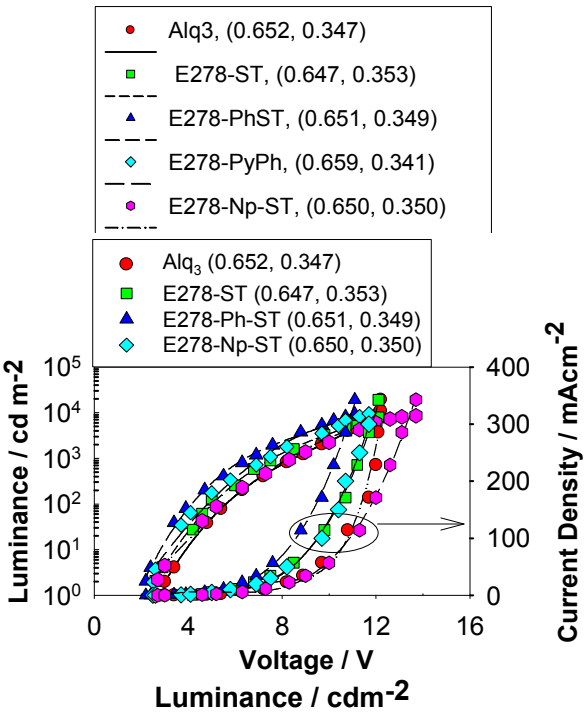

Figure 26 Current efficiency and power efficiency vs luminance plots for the red device ITO/ZnTpTP (20 nm)/α-NPB (60 nm)/Alq_3: Rub: DCJTI (30:30:0.7 nm)/ETL (30 nm)/LiF (0.5 nm)/Al

DCJ Current density vs voltage plots (Fig. 25) show that E278-

Ph-ST seems to have the most efficient current injection, followed by E278-Pyr-ST, then E278-ST. E278-Np-ST is surprisingly less effective in terms of current injection and only as good as Alq_3. Luminance vs voltage (Fig. 25) follows the same trend. However, current efficiency of the devices at 1000 cdm^{-2} shows that the efficiency of the devices with E278-Ph-ST (4.5 ± 0.1 cd A^{-1}) is comparable to that with E278-Np-ST (4.6 ± 0.1 cd A^{-1}) despite their differences in the HOMO-LUMO levels (Fig. 26).

The current efficiency follows the order E278-Np-ST =E278-Ph-ST > Alq_3 >E278-Pyr-ST > E278-ST. Power efficiency follows the order E278-Ph-ST > E278-Np-ST > E278-Pyr-ST > Alq_3 > E278-ST (Fig. 26).

Turn-on voltage (Vt) for all the E278-X (X= E278-ST, E278-Ph-ST, E278-Np-ST, E278-Pyr-ST) derivatives are all comparable (2.1 ± 0.2 V, slightly higher than the band gap of DCJTi, 2.06 eV) and much lower than the turn-on voltage when Alq_3 (3 V) was used as electron transport layer. The operating voltage to achieve 1000 cd m^{-2} follows the following order: E278-Ph-ST (6.2 ± 0.1 V) < E278-Pyr-ST (7.2 ± 0.1 V) < E278-ST (7.5 ± 0.1 V) < E278-Np-ST (8.0 ± 0.1 V) = Alq_3 (8.2 ± 0.1 V).

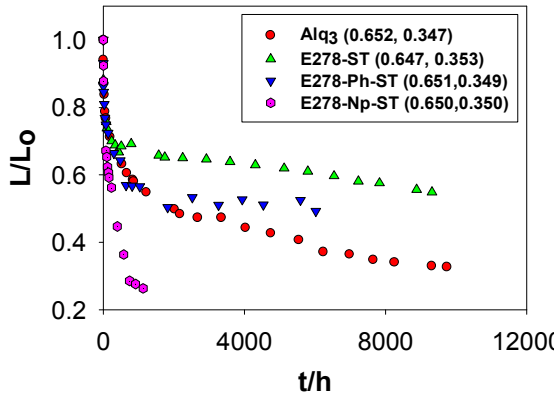

Figure 27 Lifetime plots for the red device ITO/ZnTpTP (20 nm)/α-NPB (60 nm)/Alq_3: Rub: DCJTI (30:30:0.7 nm)/ETL (30 nm)/LiF (0.5 nm)/Al at 500 cdm^{-2}

Lifetime studies (Fig. 27) were carried out on the red devices at initial luminance of 500 cd m^{-2} at constant current and voltage drift plots for the same devices (drift voltage normalised with respect to Alq_3) are given in Fig. 28.

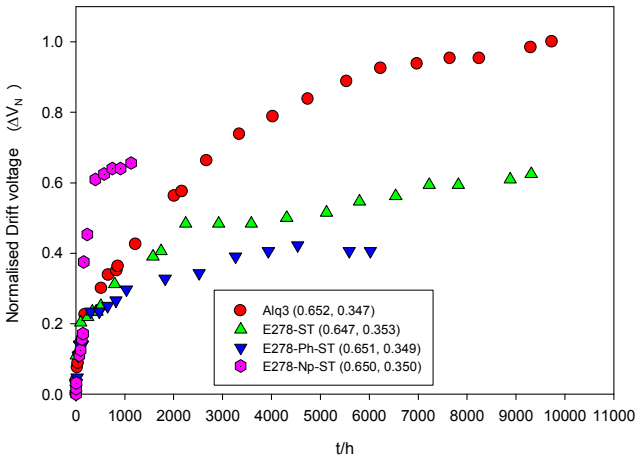

Figure 28 Voltage drift plots of the red devices ITO/ZnTpTP (20 nm)/α-NPB (60 nm)/Alq_3: Rub: DCJTI (30:30:0.7 nm)/ETL (30 nm)/LiF (0.5 nm)/Al

The lifetime of only E278-ST, E278-Ph-ST and Alq_3 were measured. Devices with E278-Np-ST were not stable at 500 cd m^{-2}. The half-life of the devices with Alq_3, E278-ST and E278-Ph-ST as etl were found to be 2000 hours, 10000 hours and 6500 hours. The lifetime of the devices with E278-ST and E278-Ph-ST is five times and nearly three times the lifetime of Alq_3, respectively.

Normalised voltage drift after 6500 hours of operation was found to be 0.93, 0.58, 0.40 for Alq_3, E278-ST and E278-Ph-ST as etl indicating that the E278-ST and E278-Ph-ST based devices are more stable than Alq_3.

Electron transporting characteristics of E278-X in green devices

DPQA

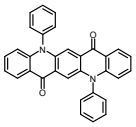

Figur e 29 Energ y level diagra

	V_t on /V (a)	V_{op} /V (b)	CIE (		ency (b)
Alq_3	4.5 ± 0.1	9.5 ± 0.1	(0.32		
E278-ST	3.9 ± 0.1	8.5 ± 0.1	(0.29		
E278-Ph-ST	3.9 ± 0.1	8.6 ± 0.1	(0.297, 0.666)	7.0 ± 0.5	2.3 ± 0.2
E278-Th-ST	3.5 ± 0.1	8.5 ± 0.1	(0.320, 0.647)	7.5 ± 0.5	3.0 ± 0.2
E278-Np-ST	3.0 ± 0.1	8.5 ± 0.1	(0.288, 0.670)	12.5 ± 0.5	4.0 ± 0.2
E278-PyR-ST	3.2 ± 0.1	10.5 ± 0.1	(0.317, 0.651)	11.0 ± 0.5	3.0 ± 0.2

(a) at 1 cd m^{-2} (b) at 1000 cd m^{-2}

m for device structure: ITO/ZnTpTP (50 nm)/α-NPB (50 nm)/Alq_3: DPQA (50:0.1 nm)/ETL (20 nm)/LiF (0.5 nm)/Al

Green devices were manufactured with DPQA as the dopant and Alq_3 as the host. The device structure was ITO/ZnTpTP (50 nm)/α-NPB (50 nm)/Alq_3: DPQA (50 nm: 0.1 nm)/ETL (20 nm)/LiF (0.5 nm)/Al (See Fig. 33) where the ETL were E278-ST, E278-Ph-ST, E278-Th-ST, E278-Np-ST, E278-Pyr-ST and Alq_3 and their performance are shown in Table 10.

The current density vs voltage plot (Fig. 30) reveals that all the E278-X derivatives have higher current injection ability than Alq_3 and the differences among them is small, although a trend of E278-Ph-ST > E278-Th-ST > E278-Np-ST > E278-Pyr-ST > E278-ST > Alq_3 can be gleaned. The luminance vs voltage plot (Fig. 30) gives a slightly different order, but the differences between the E278-X derivatives are small. They all have considerably lower operating voltage than Alq_3 as electron transport layer.

Table 10 Performance data of the green devices. Device structure: ITO/ZnTpTP (50 nm)/α-NPB (50 nm)/Alq_3: DPQA (50: 0.1 nm)/ETL (20 nm)//LiF (0.5 nm)/Al

Figure 30 Current density and luminance vs voltage plots of the green devices. Device structure: ITO/ZnTpTP (50 nm)/α-NPB (50 nm)/Alq_3: DPQA (50:0.1 nm)/ETL (20 nm)/LiF (0.5 nm)/Al

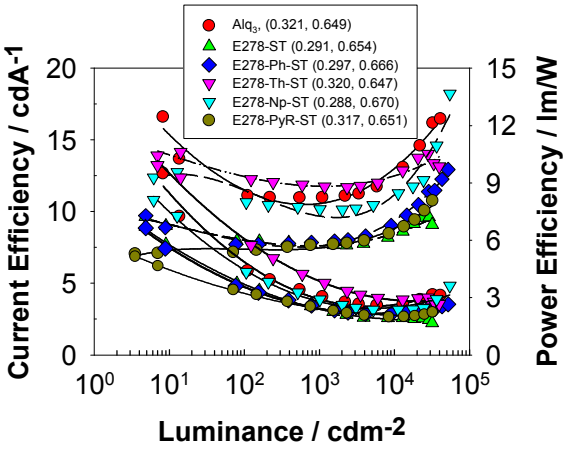

Figure 31 Current efficiency and power efficiency vs luminance plots of the green devices. Device structure: ITO/ZnTpTP (50 nm)/α-NPB (50 nm)/Alq_3: DPQA (50:0.1 nm)/ETL (20 nm)/LiF (0.5 nm)/Al

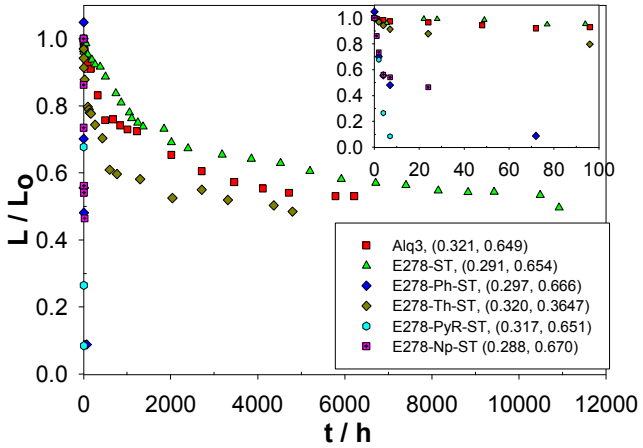

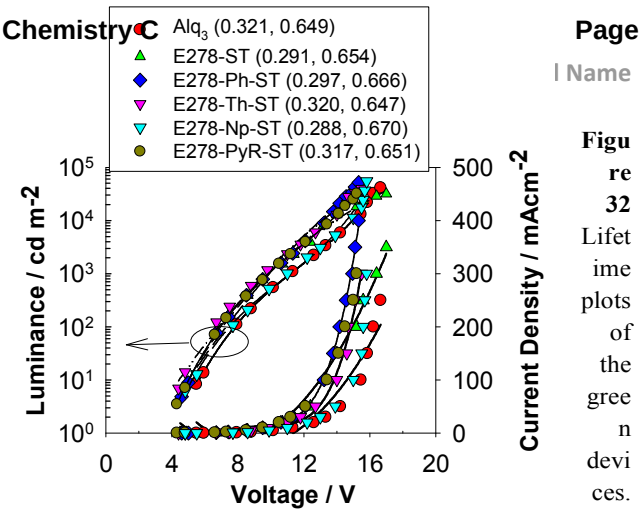

Figure 32 Lifetime plots of the green devices. Device structure: ITO/ZnTpTP (50 nm)/α-NPB (50 nm)/Alq_3: DPQA (50:0.1 nm)/ETL (20 nm)/LiF (0.5 nm)/Al at the initial luminance of 1200 cd m^{-2}

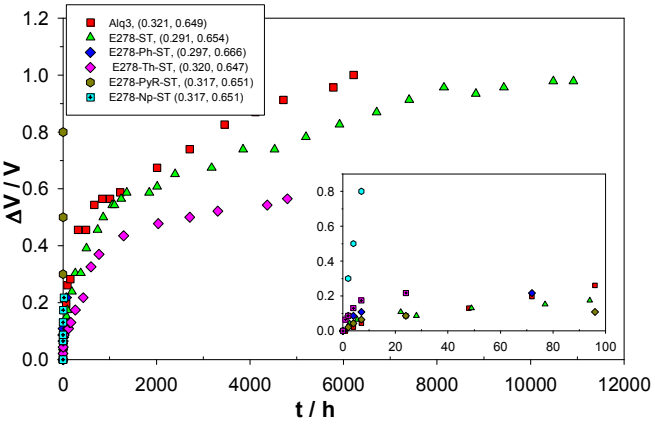

Figure 33 Voltage drift plots of the green devices. Device structure: ITO/ZnTpTP (50 nm)/α-NPB (50 nm)/Alq_3: DPQA (50:0.1 nm)/ETL (20 nm)/LiF (0.5 nm)/Al

E278-X as blue emitters

Since E278-X are highly blue fluorescent in solvents such as dichloromethane, chloroform and acetonitrile as well as in thin films, we decided to investigate the properties of E278-ST, and E278-Ph-ST as dopants using 1,3-bis(N-carbazolyl)benzene (m-CP) as a host. $BAlq_2$ was used as the etl.

We fabricated devices of the structure ITO/MoO_3 (10 nm)/α-NPB (40 nm)/mCP: E278-x (50 nm: 1 nm)/$BAlq_2$ (10 nm)/LiF (0.5 nm)/Al (Fig 34).

The EL spectra (λ_{max}, 439 nm) of the devices with E278-ST as the dopant overlaps completely with the PL of 2% doped E278-ST in m-CP thin films produced by VTE (Figure 35). This indicates that the excited state involved the EL is identical to that in the PL. The devices emitted purplish blue colour (CIE, (x,y): (0.156, 0.112). The current and power efficiencies of the devices were 0.4±0.1 cd/A and 0.1 lm/W at 1000 cdm^{-2} respectively.

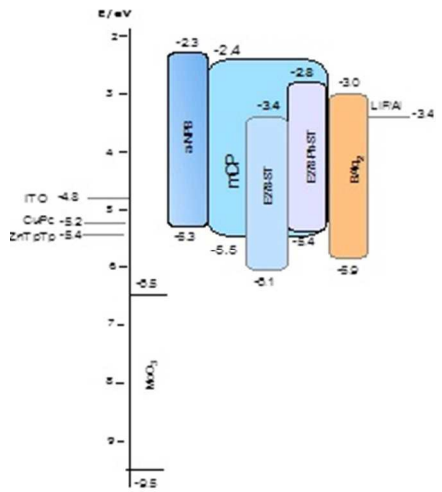

Figure 34 Energy level diagram for the device structure: ITO/MoO_3 (10 nm)/α-NPB (40 nm)/mCP: E278-X (50: 1 nm)/$BAlq_2$ (10 nm)/LiF (0.5 nm)/Al

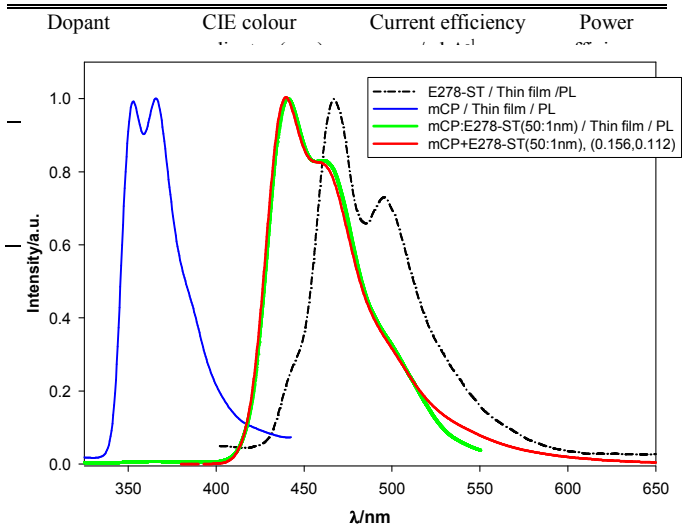

Figure 35 The EL spectra of devices where E278-ST is the dopant and the PL spectra with 2 % E278-ST as dopant

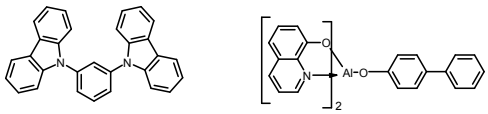

mCP $BAlq_2$

The EL spectra of the devices based on E278-Ph-ST is similar to that of PL (λ_{max}, 456 nm, shoulder 470 nm), but the PL has an additional shoulder at 410 nm, akin to the features of the PL obtained from pure (neat) E278-Ph-ST films produced by VTE (Figure 36). We therefore conclude that the excited states involved in both cases are same. E278-Ph-St devices show higher efficiencies (1 cd/A, 0.2 lm/W at 1000 cdm^{-2}), but dark blue emission (CIE, x,y: 0.164, 0.186) (Figure 37). We believe that the optimisation of the thickness of the hole transporter, emissive layer and the dopant level should result in higher efficiency. This work is ongoing and will be published elsewhere.

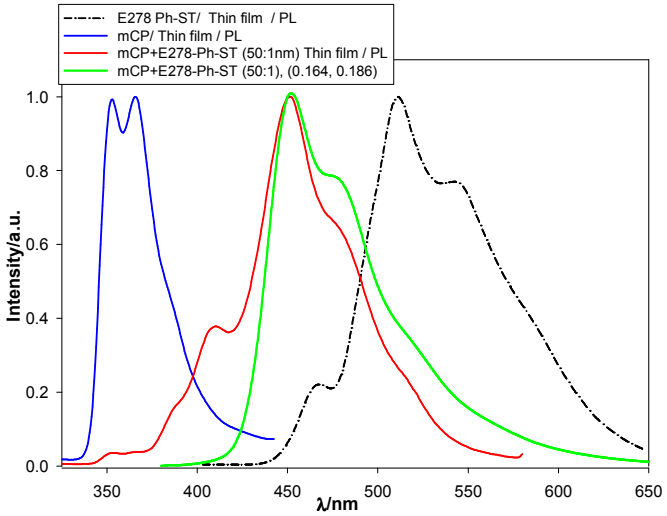

Figure 36 The EL spectra of devices where E278-Ph-ST is the dopant and the PL spectra with 2 % E278-Ph-ST as dopant

Table 11 Performance data of the blue devices. Device structure: ITO/MoO_3 (10 nm)/α-NPB (40 nm)/m-CP: E278-X (50: 1 nm)/$BAlq_2$ (10 nm)//LiF (0.5 nm)/Al

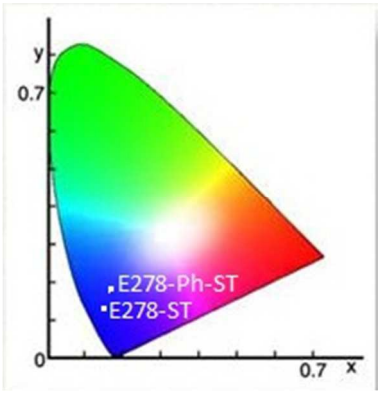

Figure 37 CIE coordinates of the EL of the blue devices of ITO/MoO_3 (10 nm)/α-NPB (40 nm)/mCP: E278-X (50: 1 nm)/$BAlq_2$ (10 nm)/LiF (0.5 nm)/Al

CIE colour coordinate diagram in Figure 36 illustrates the colour obtained from the E278-ST (purple blue) and E278-Ph-ST (blue) devices.

Conclusions

A number of thermally stable, conjugated, blue emitting vinylene bis(vinyl quinolinyl)benzene derivatives were prepared and three of them were characterised by single-crystal X-ray crystallography. They exhibit blue to bluish-green emission (fluorescence and electroluminescence) depending on their substituents. We have demonstrated that band gaps, HOMO-LUMO levels and the mobilities can be tuned by appropriate choice of substituents. Some derivatives namely E278-ST, E278-Ph-ST and E278-Th-ST leave no residues on vacuum thermal evaporation.

Their effectiveness as electron transporters in red and green OLEDs has been explored. The phenyl- and naphthyl-substituted compounds were found to be superior to Alq_3 as electron transporters in organic light emitting diodes (OLEDs). The electron mobility of the parent molecule and its phenyl-, thienyl- and naphthyl-substituted compounds were determined to be 8×10^{-7}, 3.3×10^{-6}, 5.5×10^{-6} and 8×10^{-6} respectively.

The dark blue electroluminescence from the E278-ST and E278-Ph-ST derivatives opens up an area of colour tuning from simple molecular modification.

Supplementary information

The 6-substituted 2-methyl-8-hydroxyquinoline was synthesised by Suzuki coupling reaction from 6-bromo-2-methylquinolines and the corresponding boronic acids. Bis(vinyl quinolinyl)benzene derivatives were made by refluxing benzene-1,4-dicarboxaldehyde (terephthalaldehyde) with the 2-methylquinolinyl derivative in acetic anhydride and subsequent purification by sublimation. The synthetic details of the compounds presented are given in the Supplementary Information.

Notes and references

[a] Organic Electronics, Wolfson Centre, Brunel University London, Kingston Lane, Uxbridge, UB8 3PH, UK. p.kathirgamanathan@brunel.ac.uk
[b] School of Chemistry, University of Nottingham, University Park, Nottingham, NG7 2RD, UK.
a.j.black@nottingham.ac.uk

1. (a) H.Sasabe and J. Kido, *J of Mater. Chem C*., 2013, 1, 1699-707; (b) J. W. Kwon, T. J. Park, W. S. Jeon, S. H. Jeon, J. J. Park, Y. K. Lee and J. Jang, *SID Symposium Digest of Tech. Papers*, 2007, 38(1), 888-891; (c) P. Kathirgamanathan, S. Surendrakumar, J. Antipan-Lara, S. Ravichandran, V.R. Reddy, S. Ganeshamurugan, M. Kumaraverl, V. Arkley, A. J. Blake and D. Bailey, *J. Mater. Chem*., 2011, **21**, 1762-1771; (d) P. Kathirgamanathan, S. Surendrakumar, S. Ravichandran, R. R. Vanga, J.Antipan-Lara, S. Ganeshamurugan, M. Kumaraverl, G. Paramaswara and V. Arkley, *Chem. Lett.,* 2010, **39**, 1222-1224; (e) P. Kathirgamanathan, S. Surendrakumar, R. R. Vanga, S. Ravichandran, J. Antipan-Lara, S. Ganeshamurugan,M. Kumaraverl, G. Paramaswara and V.Arkley, *Organic Electronics*, 2011, **12**, 666-676; (f) S. Chen, J. Wei, K. Wang, D. Chen, Y. Liu and Y. Wang, *J. Mater. Chem.*, 2013, 1, 6594-6602; (g) P. Kathirgamanathan and S. Surendrakumar, *Patent* (PCT)., WO2009/112854 A1 (17-09-2009)
2. (a). P. Kathirgamanathan, V. Arkley, S. Surendrakumar, G. Paramaswara, J Antipán-Lara, S. Ravichandran, S. Ganeshamurugan, M. Kumaraverl and Y. F. Chan, *Asian Soc. for Information Display*, 2007, ISBN: 978-981-05-8143-5. (2b). P. Kathirgamanathan, S. Surendrakumar, Juan Antipan-Lara, S. Ravichandran, Y.F.Chan, V. Arkley, S. Ganeshamurugan, M. Kumaraverl, G. Paramaswara, A. Parteepan, V. R. Reddy, D. Bailey and A. J. Blake, J. Mater. Chem.,2012, 22, 6104-6116.
3. K. Ueno, A. Senoo and S. Mashmo, *US Patent*. 6436559B1, 20-08-2002.
4. S. H. Son, O. K. Kim, S. H. Yoon, K. K. Kim., Y. G. Lee and J. S. Bae, *US Patent*. 6720573B2, 13-04-2004.
5. K. P. Klubeck and D. Y. Kondakov, *US Patent*. 2007/0122657, 31-05-2007.
6. P. Kathirgamanathan, V. Kandappu, S. Hara, K. Chandrakumar, S. L. Marianesan, S. Selvaranjan, S. Surendrakumar and M. J. Toohey, *Mater. Lett.*, 1999, **40**, 285.
7. S. Reinnke, F. Lindner, G. Schwartz, N. Seidler, K. Walzer, B. Lussem and K. Leo, *Nature*, 2009, 459, 234.
8. H. Sasabe, T. Chiba, S. J. Su, Y-J. Pu, K. Naayama and J. Kido, *Chem., Commun.,* 2008, 5821.
9. J. J. Brown, *IMID,* OLED Workshop, Korea, 2007.
10. (a) J. Endo, T. Matsumoto and J. Kido, *Jpn. J. Appl. Physics*., 2002, **41,** L358; (b) P. Kathirgamanthan, S. Surendrakumar, S. Ravichandran, R.V. Reddy, J. Antipan Lara, S. Ganeshamurugan, M. Kumaraverl, G. Paramaswara and V. Arkley, *Chem Letts*., 2010, 122-124; (c) A. P. Kulkarni, C. J. Tonzole, A. Babel and S. A. Jeneke, *Chem. Mater*., 2004, **16**, 4556; (d) G. Hughes and M. R. Bryce, *J. Mater. Chem., 2005*, **15**, 94-107
11. I. D. Parker, *J. Appl. Phys.*, 1994, **75**, 1656.
12. (a) A. J. Heeger, I. D. Parker and Y. Yang, *Synthetic Metals.*, 1994, **67,** 23; (b) D. R. Baigent, N. C. Greenham, J. Gruner, R. N. Marks, R. H. Friend, S. C. Moratti and A. B. Homes, *Synthetic Metals.,* 1994, **67**, 3-10
13. R. Partridge, *US Patent.* 1976/ 3995299
14. C. W. Tang, *US Patent*. 1982/ 4356429
15. C. W. Tang and S. A. VanSlyke, *Appl. Phys. Lett*., 1987, **51**, 913.
16. J. H. Burroughes, D. D. C. Bradley, A. R. Brown, R. N. Marks, K. Mackay, R. H. Friend, P. L. Burn and A. B. Holmes, *Nature*, 1990, **347,** 539.
17. J. Kido, K. Nagai and Y.Okamoto, *IEEE Trans. Electron Devices*, 1997, **44**, 1245.
18. T. Wakimoto, Y. Fukuda, K. Nagayama, A. Yokoi, H. Nakada and M. Tsuchida., *IEE Trans. Electron Devices*, 1997, **44**, 1245.
19. P. Kathirgamanathan and D. R. Rosseinsky, *J. Chem. Soc., Chem. Commun*., 1980, 839.
20. L. B. Valdes, Proc. I.R.E., 1954, **42**, 420.
21. L. J. Van der Pauw, *Philips Research Reports.*, 1958, **13**, 1.
22. L. J. van der Pauw, *Philips Tech. Reviews*, 1959, **20**, 220.
23. L. J. Van der Pauw, *Philips Research Reports*, 1961, **16,** 187.
24. P. Kathirgamanathan, *Ph. D Thesis* (Exeter)-(1980)
25. Physics and Chemistry of the Organic Solid State, Editors: D. Fox, M.M. Labes, A. Weissberger, Interscience Publishers, New York (1967).
26. B. W. D'Andrade, S. Datta, S. R. Forrest, P. Djurovich, E. Polikarpov and M. Thmpson, *Organic Electronics,* 2005**, 6**, 11.
27. M. Cole and W. Brutting, Physics of Organic Semiconductors, pages 95-128, Wiley-VCH Verlag GmBH, ISBN-13: 978-3-527-40550-3 (2005).
28. S. J. Su, H. Sasabe, Y.J Pu, K.Nakayama and J. Kido, *Adv. Mater*., 2010 **22**,3311.
29. K. T. Kamtekar, A. P. Monkman and M. R. Bryce, *Adv. Materials*., 2010, **22**(5), 572-582
30. (a) S. Hyun Kim, J. Jang and J Y. Lee, *Appl. Phys. Letts*., 2007, 91, 083511; (b) S. Ok Jeon, K S. Yook, C, W, Joo and J. Y. Lee, *Adv. Materials.*, 2010, **22**(16), 1872
32. (a) J. Antipan Lara and P. Kathirgamanathan, *IEEE Proc. Optoelectron*., 2000, 147, 369; (b) D. R. Lamb, Electrical conduction Mechanisms in Thin Insulating Films., 1967, Methuen and Co. Ltd, 11, New Felter Lane, London EC4
33. D. Yokahama, *J. Mater. Chem*, 2011, **21**, 19187-19202
34. Agilent Technologies, 10 Mead Road, Yarnton, Oxfordshire OX5 1QU, United Kingdom
35. G. M. Sheldrick, *Acta Crystallogr., Sect. A* 2008, **64**, 112.
36. G. M. Sheldrick, *Acta Crystallogr., Sect. A* 2015, **71**, 3.
37. L. J. Bourhis, O. V. Dolomanov, R. J. Gildea, J. A. K. Howard and H. Puschmann, *Acta Crystallogr., Sect. A* 2015, **71**, 59.
38. C. F. Macrae, P. R. Edgington, P. McCabe, E. Pidcock, G. P. Shields, R. Taylor, M. Towler and J. van de Streek, *J. Appl. Crystallogr*. 2006, **39**, 453.

39.

a. S. R. Butter, Ph. D. Thesis, "Effects of Conformation on the Electronic and Optical Properties of Aryleneethylenes" Durham University (2007).
b. L. D. Bozano, B. W. Kean, V. R. Deline, J. R. Salem and J. C. Scott, Appl. Phys. Letters, 84 (4), 607 (2004).
c. Z. S. Su, M. K. Fung, C. S. Lee, W. L. Li and S. T. Lee, Appl. Phys. Letters, 93, 083301 (2008).
d. M. A. Mohd Sarjidan, S. H. Basri, N. K. Zaaba, M. S. Zainin and W.H. Abd Majid, Bulletin of Materials Science, 2015, 38(1), 235-239.
e. Y.K. Fang, Y.T. Chiang, S.F. Chen, C.Y. Lin, S.C. Hou, C.S. Hung, T.W. Tsai, S.H. Chang and T. H. Chou, J. Physics and Chemistry of Solids, 69 (2008) 738-741
f. T.Y. Chang, Y. W. Cheng and P.T. Lee, Appl. Phys. Letters, 96, 043309 (2010).
g. Y. S. Kim, S.Y. Jung, K. H. Koh and S. Lee, J. Korean Physical Society, 53 (6), 3563 (2008)